July 2007

Hydrodynamics of torsional probes for atomic force microscopy in liquids

Sudipta Basak
Birck Nanotechnology Center, School of Mechanical Engineering, Purdue University, sbasak@purdue.edu

Arthur Beyder
Department of Physiology and Biophysics, University at Buffalo, State University of New York

Chiara Spagnoli
Department of Physiology and Biophysics, University at Buffalo, State University of New York

Arvind Raman
Department of Physiology and Biophysics, University at Buffalo, State University of New York, raman@purdue.edu

Fredrick Sachs
Department of Physiology and Biophysics, University at Buffalo, State University of New York

Hydrodynamics of torsional probes for atomic force microscopy in liquids

Sudipta Basak
School of Mechanical Engineering and the Birck Nanotechnology Center, Purdue University, 585 Purdue Mall, West Lafayette, Indiana 47907, USA

Arthur Beyder and Chiara Spagnoli
Department of Physiology and Biophysics, University at Buffalo, State University of New York, 3535 Main Street, Buffalo, New York 14214, USA

Arvind Raman[a)]
School of Mechanical Engineering and the Birck Nanotechnology Center, Purdue University, 585 Purdue Mall, West Lafayette, Indiana 47907, USA

Fredrick Sachs
Department of Physiology and Biophysics, University at Buffalo, State University of New York, 3535 Main Street, Buffalo, New York 14214, USA

(Received 16 April 2007; accepted 8 June 2007; published online 26 July 2007)

Improving the force resolution of atomic force microscopy for soft samples in liquid requires soft cantilevers with reduced hydrodynamic cross section. Single and dual axis torsion levers [Beyder and Sachs, 2006] are an attractive technology. They have reduced area and reduced drift due to the symmetric support [Beyder *et al.*, 2006] can add a second dimension using two independent axes. Here we investigate the hydrodynamics of these probes using three-dimensional transient fluid-structure interaction models with comparison to the experimental data. The computed Q factors and wet/dry resonance frequencies of different modes compare well with experimental measurements indicating that continuum viscous hydrodynamics can be used effectively to predict probe performance. The modeling further explores cross-axis hydrodynamic coupling and the influence of a nearby sample plane to provide guidance on approach algorithms and the possibilities of parametric detection. © *2007 American Institute of Physics*. [DOI: 10.1063/1.2759197]

I. INTRODUCTION

Atomic force microscopy (AFM) is a unique tool to probe the mechanical properties of hydrated biological samples including live cells and of single biopolymers in normal saline.[1–3] Efforts to improve the force resolution and sensitivity of AFM probes in liquid environments, however, require fundamentally different probe designs that offer simultaneously (a) low stiffness, (b) low thermal noise, and (c) reduced hydrodynamic cross sections.

Reduced probe stiffness is required because biological samples are often soft relative to the stiffness of cantilevers.[4–6] Thus, sample compliance can be a minor perturbation of the cantilever compliance. However, reducing cantilever stiffness without reducing its mass significantly is not the correct solution either, since it leads to reduced resonance frequencies (response times) and greater thermal noise.

The ultimate limit of force or displacement resolution of the AFM probe is set by thermal noise with an energy of $(1/2)k_BT$=4.1 pN nm per degree of freedom at room temperature. The root-mean-square thermal noise can be reduced by low pass filtering, since in the frequency domain the noise is spread over the bandwidth of the cantilever. For a given low-frequency passband, the higher the probe resonance frequency (and Q factor) the lower the noise. With a fixed bandwidth, stiffer cantilevers will provide higher resolution, but they are more prone to producing sample damage upon approach.

The only way to reconcile the earlier seemingly contradicting requirements is to reduce the probe stiffness and reduce significantly its oscillating mass and hydrodynamic cross section. This can lead to probes that are simultaneously low stiffness and yet high frequency (low thermal noise when a low band pass filter is used) and high bandwidth. The response time (resonance frequency) of probes in liquid environments, however, is dictated by the viscous dissipation and added inertia of the water. For soft commercial levers ~0.01 N/m, the bandwidth is typically <1 kHz. Making short narrow cantilevers can reduce the hydrodynamic loading,[7] but places demands on the optics, requiring the laser beam to be focused on a small area. Moreover, the residual stresses in the cantilever can cause warping of the cantilever plane.

Torsional AFM probes are a new class of AFM probes that not only address the earlier technical challenges, but also offer several additional advantages. Beyder and Sachs[8] fabricated relatively small (~20 μm), symmetrically supported torsion levers that had <10% of the area of commercial cantilevers and fit standard AFMs. Support symmetry nearly eliminated drift due to changes in hydration and temperature.[9] These cantilevers were made with spring constants <0.01 N/m and frequency response >10 kHz in water with an underdamped resonance, and there was only one

[a)]Electronic mail: raman@ecn.purdue.edu

significant vibrational mode. Being short, ~10 μm from tip to hinge axis, the optical gain increased >10×, so that a given z deflection will produce a larger optical signal. This allows the use of stiffer cantilevers with higher bandwidth, or equivalently, a lower noise in a fixed bandwidth. For friction imaging, locating the tip over the tilt axis provides a large increase in sensitivity over convention levers. Since the pad that supports the tip and forms the mirror for the optical lever is rigid, there is no curvature during bending and magnetic films, as used in the magnetically excited mode, will not distort the mirror.[8]

The microfabrication techniques for the single axis probe were applied to a two axis gimbaled probe where the two orthogonal axes provide independent data channels that can be exploited in many ways. One axis can be used to encode the substrate position and the other the sample position, thereby removing microscope drift. All common mode noise sources such as building vibration, low frequency acoustic noise, and laser power fluctuations will also be eliminated. Since the observed compliance of a sample in AFM is really the compliance of the cantilever plus the sample, when the two axes have different stiffness, we have two simultaneous equations for the sample compliance, and can solve for the sample compliance in real time. The cross correlation of the two axes (at different frequencies) can provide information about the anisotropic properties of the sample.

In spite of the tremendous potential of single and dual axis torsion probes for highly sensitive force spectroscopy and imaging, the hydrodynamics of these probes are not well understood. Existing methods to compute hydrodynamic loading assume the levers are long and slender[10–12] and are inapplicable to torsion probes. An improved understanding of torsion probe hydrodynamics can lead to design guidelines for (a) maximizing Q factors and resonance frequencies in these probes, (b) predicting the variation of Q factors with cantilever proximity to sample thereby enabling new approach algorithms, (c) choosing tip lengths so that cantilever modes remain underdamped upon approach to sample surface, and (d) dual-axes probes with minimal hydrodynamic coupling between the torsion axes.

The goal of this article is to investigate the hydrodynamic interactions of single and dual axes levers using experimental measurements and transient, fully three-dimensional fluid-structure interaction models.[13] Of particular interest are the influence of a nearby sample plane and on the cross-axis hydrodynamic coupling arising from fluid momentum coupling. The theoretical predictions are compared to experimental results and found to be in good agreement proving that continuum viscous hydrodynamics can be used to understand the physics of torsional probe oscillations in liquids. In principle, the approach can be extended to predict the lever response when approaching asymmetric elastic substrates. The results provide a comprehensive understanding of hydrodynamic effects in torsion levers and lay the ground rules for further improvements in their design.

II. SIMULATION METHODS

We model the symmetric and asymmetric single axis and dual axis torsion levers in viscous incompressible Navier–Stokes fluid using finite element model in ADINA.[14] We follow the approach of Basak *et al.*,[13] where the fluid model consists of a layer of Navier–Stokes elements around the oscillating structure, which is followed by another layer of potential based fluid elements. The potential fluid layer terminates in an infinite fluid boundary, effectively representing the oscillation of the structure in unbounded fluid.

The required hydrodynamic effects are computed using a "modal" ring-down simulation of each probe structure. For this, first a modal analysis of the structure is performed *in vacuo*. This yields the mode shapes of the structure. In the modal analysis we adjust the thickness and/or the material properties of the hinges to achieve *in vacuo* frequencies that match the experimentally measured frequencies in air. Following the *in vacuo* study, we move to the transient fluid-structure interaction code. The probe is provided an initial velocity perturbation in a direction corresponding to its *in vacuo* mode shape. This ring-down procedure ensures that only the chosen mode participates in the response, allowing the single-degree-of-freedom oscillator theory to model the transient. Fitting the transient response yields the Q factor and the resonance frequency. (For details of using transient oscillations to quantify Q and resonance frequency, see Ref. 13).

One important aspect for the dual-axis levers [Fig. 1(b)] is the intrinsic mechanical and external hydrodynamic cross coupling of the two axes. Hydrodynamic coupling between neighboring micromechanical oscillators has been studied in detail;[15] our interest in the present setting is in the corresponding coupling between two axes of the same structure. Because the rotational motions about each axis are weakly coupled in air, each *in vacuo* mode described by rotation about one specific axis also contains a small rotation about the orthogonal axis. This coupling is computed by evaluating the ratio of orthogonal rotations in each mode. In water, however, the coupling is stronger and the model is expanded to include hydrodynamic correlations as described in Sec. IV B.

We also compute the frequencies, Q factors, and cross-axis coupling when the dual axis lever (Q3G) vibrates close to a surface to mimic practical operation of the AFM. In this case, the fluid domain below the lever is replaced by a rigid wall in close proximity, and the "ring-down test" described earlier yields the required hydrodynamic quantities. Typically, Q and the natural frequency decrease in the proximity of the sample surface due to additional dissipation from squeeze film damping.[13] Results of these simulations are described in Sec. IV C.

III. EXPERIMENTAL METHODS

A. Probe fabrication

Torsion probes are manufactured using a microfabrication process previously described by Beyder and Sachs.[8] This process employs routinely available microfabrication tools and allows for the mass production of a wide variety of

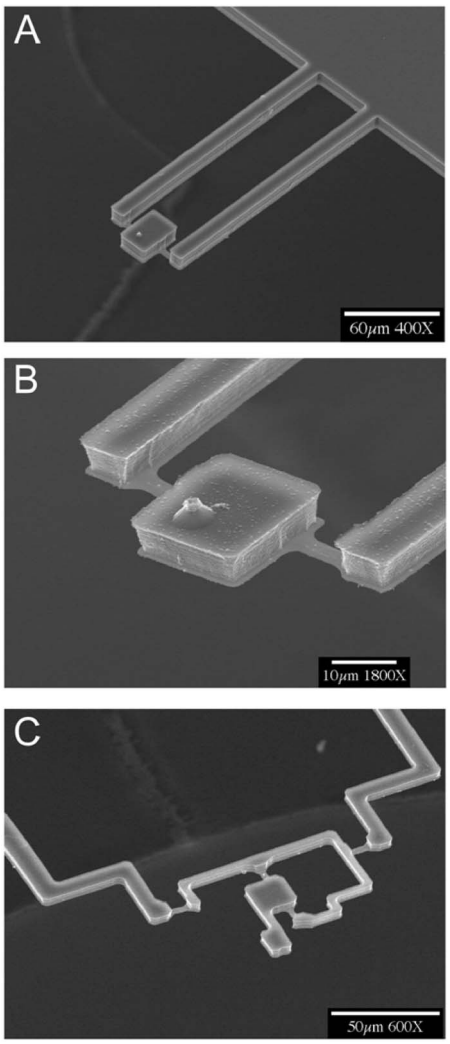

FIG. 1. SEM images of some AFM torsional probes used in this study. (a) Single-axis (TL1a) probe with a 20×40 μm silicon torsional pad is symmetrically balanced on thin SiN hinges (10×4 μm$\times75$ nm). To improve optical and physical clearance, the oscillator is extended from the handle die (not pictured) on stiff Si support bars. (b) Single-axis (TL2b) probe with an asymmetrically positioned pad (20×22 μm, 4 μm off-center). (c) Dual-axis (Q3G) torsion AFM probe.

ultrasensitive oscillators, including those pictured in Fig. 1. We fabricate levers that fit on a typical AFM with a laser beam waist of ~20 μm, so the smallest mirror/tip support pad is $\sim20\times20$ μm. Soft hinges are fabricated in order to make these short probes (10 μm from hinge to edge) highly compliant. This is achieved by fabricating very thin hinges (20–75 nm thick) of low-stress silicon nitride (SiN). Despite the high compliance (~0.01 N/m), the probes are fast ($f_{\text{water}}\sim10$ kHz). The hinges are protected during fabrication by covering them with a layer of silicon dioxide (SiO_2) until the final release. The stiff parts (handle dies, support arms, and torsion pads) are bulk fabricated using microlithography, using aqueous KOH and deep reactive ion etching. The pads and arms are approximately 1000-fold stiffer than the hinges, and at 5–10 μm thick, they are essentially inflexible. The entire structure is coated with 10 nm Cr and 40 nm Au to improve reflectivity. Device and hinge dimensions are measured using a Hitachi S-4000 scanning electron microscope (SEM).

B. Frequency measurements

The probes are removed from the support wafer with tweezers and attached to a Quesant Nomad AFM (Quesant Instruments Corporation). Angular movement of the pad is sensed by a standard optical lever and a four-quadrant position-sensitive photodetector (PSD). The PSD signals: bottom–top ($B-T$) and left–right ($L-R$) are digitized by Quesant's electronic interface unit (EIU), which allows acquisition rates up to 96 kHz. The analog displacement signals are also streamed from the EIU to an eight-pole Bessel filter (Krohn-Hite 3341) where data are filtered (0.1 Hz–99.9 kHz) and amplified ($100\times$). The amplified signal is sent to a digital oscilloscope (TDS220, Tektronix, Inc.) and a personal computer acquisition board (AT-MIO-16E2, National Instruments). The sampling frequency is set to greater than the Nyquist limit at the first-mode resonance peak. The power spectrum is also measured by the oscilloscope's internal fast Fourier transform (FFT) routine. The time-series data are saved using custom software within LABVIEW 7.0 (National Instruments) and then transformed into power spectra using the FFT function in ORIGIN 7.0 (OriginLab Corporation). Resonance spectra are parameterized by the resonance frequency f_0 and the Q factor by fitting the spectra to a Lorentzian in the software package ORIGIN.

IV. COMPUTATIONAL RESULTS AND COMPARISON WITH EXPERIMENTS

A. Single axis levers

Several different geometry probes are fabricated to explore the effect of pad area and on-center versus off-center pad placement on the hinges (Table I). The on-center pads may be used for contact measurements, since they have minimal moments of inertia and drag, while off-center pads may be necessary for tapping mode.

The geometric model for simulation comprises an elastic pad (although the pad is effectively rigid, the grid is used to mate with the fluid grid), elastic torsion hinges, and rigid support arms. Figure 2 shows an example of one such geometry (TL2a), the primary mode shape, and the fluid mesh used in the computational model. Based on a careful convergence study, it is found that the remaining structures [Fig. 1(a)] are hydrodynamically insignificant and not included.

In water, the initial velocity excitation quickly settles since the tip displacement $x(t)$ is damped by viscous dissipation. The displacement data are fitted in MATLAB (Ref. 16) to the transient response of a linear damped oscillator

$$x(t)=Xe^{-\pi f_n t/Q}\sin\left(2\pi f_n t\sqrt{1-\frac{1}{4Q^2}}\right), \tag{1}$$

where X, f_n, and Q_n are, respectively, the amplitude of vibration, undamped natural frequency, and the Q factor. The nonlinear least-squares fit uses a robust bisquare regression scheme within the Gauss–Newton algorithm. A typical fit is shown in Fig. 3.

The computational predictions in water for three different single-axis lever geometries agree with the experimentally obtained frequencies and Q factors in Table I. Reducing

TABLE I. Comparison of the finite element predictions and the experimentally obtained resonance frequencies and the quality factors of three single axis torsion levers. Hinge dimensions for all levers were: length $\times$ width $\times$ thickness = 10 μm $\times$ 4 μm $\times$ 75 nm.

Name of lever	Pad geometry	Water frequency (measured) (kHz)	Water Q (measured)	Computed water frequency (kHz)	Computed water Q
TL1	40 $\times$ 20 $\times$ 6 μm pad	12.9	1.6	14.6	2.2
TL2a	20 $\times$ 21 $\times$ 6 μm (centered pad)	29.0	1.8	39.8	2.6
TL2b	22 $\times$ 21 $\times$ 6 μm (pad 4 μm off-centered)	25.9	2.0	31	2.8

the pad area by a factor of 2 (TL2a vs TL1) decreases the moment of inertia increasing the resonance frequencies in air and water. The increased resonance frequency leads to a larger unsteady Reynolds number[13] which in turn leads to a slight increase in the Q factor. We also compare on-axis/off-axis pad placement (TL2b). Off-axis pads increase the inertial moment about the torsion axis leading to slightly decreased resonance frequencies and Q factors. Specifically, with an off-axis placement of 18% of the pad length (TL2b), the resonance frequency decreases by ~10%.

In addition to the Q factor and the natural frequencies in liquid, the model allows us to investigate the hydrodynamic dissipation mechanisms. Following Ref. 13, Fig. 4 shows the shear stress distribution (σ_{yz}) in the yz plane (along the lever axis) in water for the TL2b lever. This plot is made at a time instant just following the first complete oscillation cycle. The maximal shear stress occurs, as expected, near the edges of the pad and hinges. However, we will see later that as the probe is brought closer to a surface, additional shear stresses develop in the space between the lever plane, and the sample surface due to the so-called squeeze film effect.

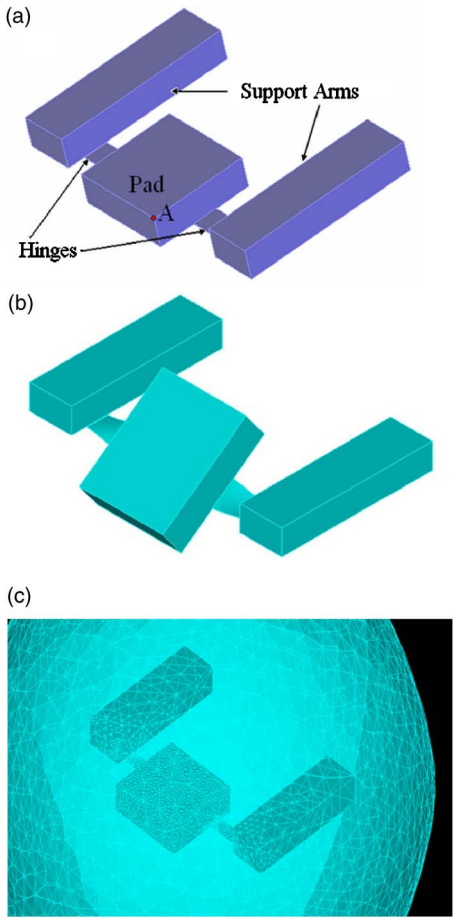

FIG. 2. (a) Schematic of the symmetric single-axis lever geometry (TL2a), (b) *in vacuo* mode shape of the single-axis lever geometry, and (c) meshed fluid model and the single-axis lever profile inside the viscous fluid. Very high mesh density is used near the pad and the hinges. The mesh density is increasingly coarser away from the pad.

B. Dual axis levers (gimbals)

We consider only one representative geometry of the two axis levers since there are many possible variations. The Q3G geometry model is shown in Figs. 1(b) and 5(a) and the structure is clamped at the two outer hinges. Since the there are two sets of torsional hinges, the first two modes are of primary importance for AFM. As before, the hinge geometry and elastic modulus are adjusted so that the *in vacuo* frequencies match those observed experimentally. The ring down for the two modes yields the different Q factors and the natural frequencies.

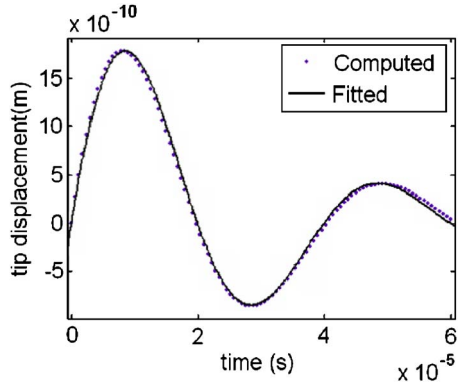

FIG. 3. Computed tip displacement data at point A on single axis lever (TL2a) during a modal ring down and the corresponding fit to the response of a single-degree of freedom oscillator. The parameters of the fit are used to determine the wet resonance frequency and the Q factor of this mode.

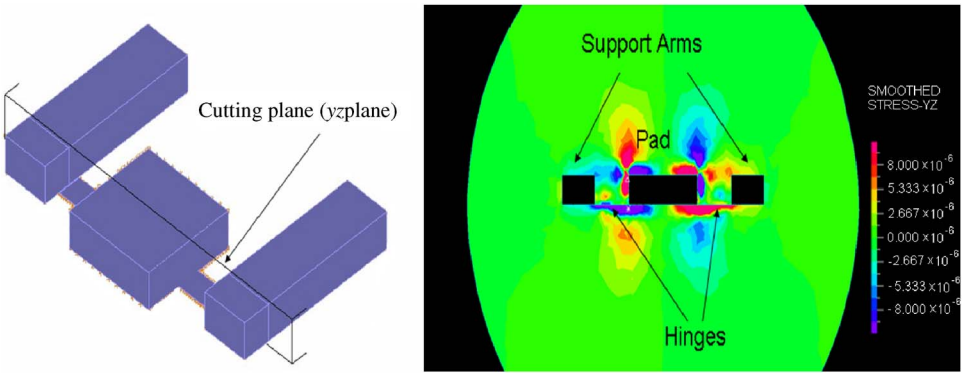

FIG. 4. (a) The cutting plane (yz plane) in the fluid domain shown with respect to the lever location. (b) Shear stress distribution (σ_{yz}) in the yz plane (along the lever axis) in the fluid for the TL2b lever vibrating in water after one cycle of oscillation. The higher shear stress concentration in the fluid around the edges of the structure indicates that most of the fluid dissipation occurs around the edges of the pad/hinges.

The first and the second mode shapes of the dual axis lever are shown in Figs. 5(b) and 5(c) respectively. In the first mode of the structure [*in vacuo* frequency 10.5 kHz, Fig. 5(b)] the entire structure rotates around the outer hinges and the outer hinges provide most of the rotational stiffness that determines frequency of this mode. Conversely, the inner hinges are mainly responsible for the stiffness of the second mode in which the main motion is the rotation of the pad around the inner hinges [*in vacuo* frequency 40.2 kHz, Fig. 5(c)] The finite element predictions of the frequencies and quality factors in water are compared with experiments in water for a dual-axis lever for the first two modes in Table II and found to be in good agreement.

As indicated before, one important aspect for the dual-axis levers is the cross coupling between the two orthogonal rotational axes. The crosstalk between the pair of hinges can be quantified as the ratio of the rotations θ_x and θ_y about the x and y axes of the structure in each mode [Fig. 5(a)]. The time dependence of θ_y, θ_x during ring down are computed from the transverse displacements of points A, B, and C [Fig. 5(a)] and are plotted in Figs. 6(b) and 6(d) for the first and the second mode, respectively. The *in vacuo* and in water cross-axes coupling are listed in Table II. The fact that the cross coupling in fluid is only slightly different from that calculated *in vacuo* indicates that external hydrodynamics modifies only slightly the intrinsic mechanical coupling between the axes. However, we will see in Sec. IV C how this hydrodynamic coupling between the two axes increases as the lever is brought closer to the surface.

C. Influence of proximity to sample on lever hydrodynamics

In this section we study the dual axis lever when it oscillates close to a surface. We replace the fluid domain below the lever by a wall at a chosen mean gap (10, 5, and 4 μm). Because the probe tip itself is 4 μm long, the probe support structure cannot be brought any closer to the sample. A similar procedure as in Sec. III B yields the hydrodynamic quantities and the results are shown in Table III. As expected,[13] the quality factors and the frequencies of the modes decrease as the lever is brought closer to the surface. Interestingly, the quality factor of the first mode of the dual axis lever drops below 0.707 when the probe-sample gap is less than 5 μm.

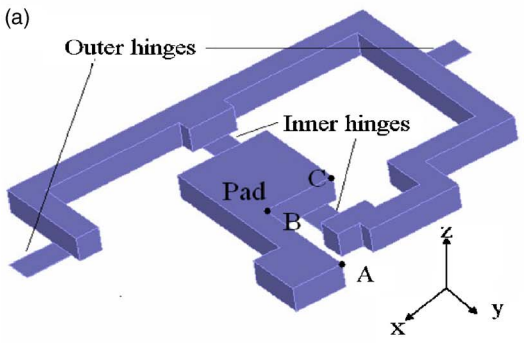

$$\theta_x = \frac{\delta(A) - \delta(B)}{AB},$$

$$\theta_y = \frac{\delta(B) - \delta(C)}{BC},$$

$$\frac{\theta_y}{\theta_x} = \begin{cases} 0.14, \text{ Mode 1 in vacuum;} \\ 0.14, \text{ Mode 1 in water;} \\ 6.7, \text{ Mode 2 in vacuum;} \\ 6.3, \text{ Mode 2 in water.} \end{cases}$$

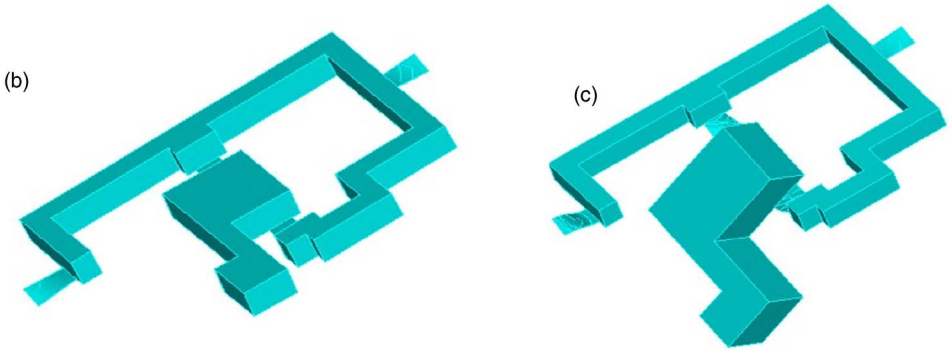

FIG. 5. (a) Schematic of the dual axis (Q3G) lever geometry. (b) First *in vacuo* mode shape of the dual axis lever. (c) Second *in vacuo* mode shape of the dual axis lever. In Fig. 4(a), $\delta(A)$ represents the transverse displacement of point A and AB represents the distance between points A and B in Fig. 4 and likewise for points B and C. From the mechanical coupling between the axes and the mode shapes we can conclude that the outer hinges are responsible of the torsional stiffness about the x axis and while the inner hinges are responsible for the torsional stiffness about the y axis.

TABLE II. Finite element predictions and the experimentally obtained resonance frequencies, quality factors, and cross-axis coupling of a dual axis torsion lever

Name of lever Q3G	Water frequency (measured) (kHz)	Water Q (measured)	Computed water frequency (kHz)	Computed water Q	Computed water θ_y/θ_x	Computed *in vacuo* θ_y/θ_x
Mode 1	5.9	0.9	5.2	1.3	0.14	0.14
Mode 2	21.5	2.3	25.7	2.0	6.3	6.7

When $Q=0.707$ for a mode it is critically damped, when $Q>0.707$ it is underdamped, and when $Q<0.707$ it is overdamped. When a mode is overdamped, there is no amplification of mechanical motion at resonance, a situation that needs to be avoided in dynamic AFM. The second mode, however, remains underdamped even at 4 μm gap length (Table III).

To fully benefit from the advantages of the dual axis levers, overdamped modes must be avoided. There are three strategies for this: (1) to use long tips, in this case at least 10 μm, to keep the lever away from the sample surface, or (2) to increase the resonance frequencies of the modes by altering hinge properties, or (3) to incline the lever relative to the sample. Higher resonance frequencies lead to smaller unsteady boundary layers;[13] as a consequence the lever can be brought closer to the sample without "feeling" the hydrodynamic influence of the sample. To demonstrate this we perform simulations using a hypothetical Q3G dual axis lever whose hinge elastic modulus has been increased ten times compared to the earlier simulation. Adjusting hinge thickness for stiffness is controllable in the fabrication procedure. The stiffer hinge results in an *in vacuo* frequency of 33 kHz. Indeed, we find that the quality factor of the lowest mode of this hypothetical at a gap of 5 μm is underdamped (Table III).

The cross-coupling terms are computed from ring-down simulations performed near the surface and shown in Table III. As the lever is brought closer to the surface, the ratio (θ_y/θ_x) for mode 1 increases while that for mode 2 decreases indicating that the wall proximity influences the cross coupling in different ways depending on the mode of oscillation. This is a somewhat nonintuitive result that underscores the importance of considering the effect of the nearby surface in the observed response.

V. DISCUSSION AND CONCLUSIONS

This work shows that state-of-the-art fluid-structure interaction codes predict well the unsteady hydrodynamics of oscillating torsion probes for AFM in liquids. The computational approach sheds light on the mechanisms of hydrodynamic dissipation and allows the torsion probes to be designed for optimal performance prior to microfabrication. Specifically we show that hydrodynamic dissipation arises

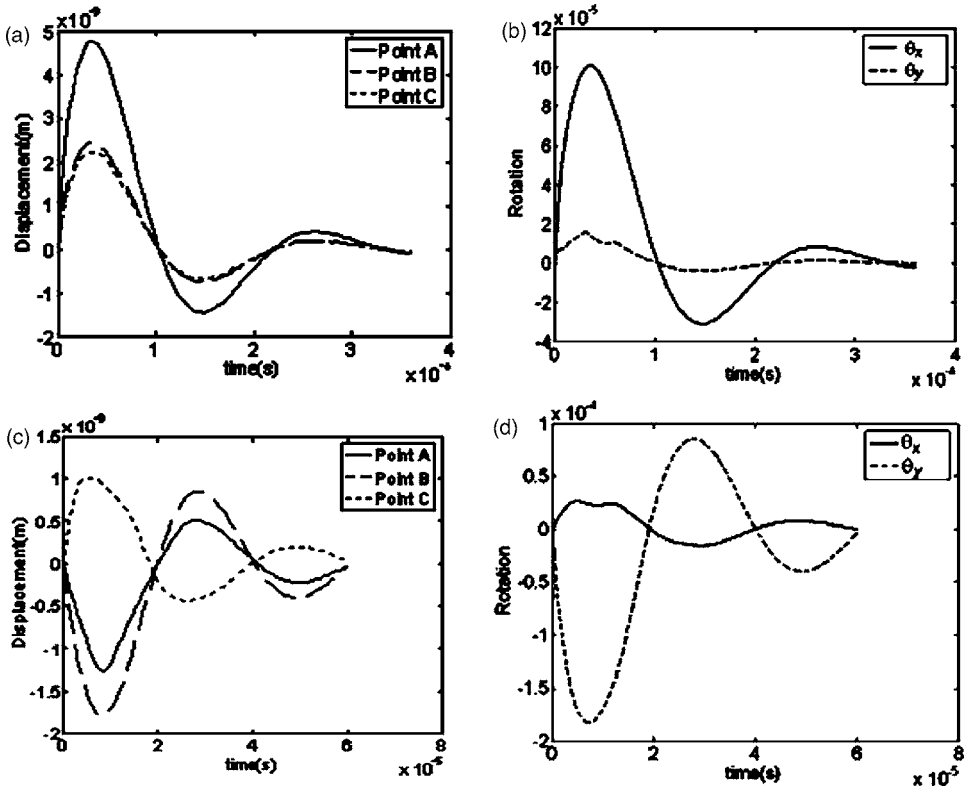

FIG. 6. (a) and (c) Plot of the displacement time histories of points A, B, and C (see Fig. 5) for the first and the second mode, respectively, and (b) and (d) the rotation time histories in the first and the second mode, respectively.

TABLE III. Computationally predicted resonance frequencies, quality factors, and cross-axis coupling of the dual axis torsion lever [Fig. 1(b)] close to a surface. Values are not provided $Q<0.5$ as there are no oscillations in the transient response. The simulations with ten times higher elastic modulus demonstrates that increased frequency (stiffness) of the probe can prevent overdamping of modes near the sample surface.

	Mode 1				Mode 2				Mode 1 ($10\times E$)		
Gap (μm)	∞	10	5	4	∞	10	5	4	10	5	4
Q	1.3	0.77	⋯	⋯	2.0	1.8	1.0	0.72	1.5	0.72	0.54
f_n (kHz)	5.2	5.1	⋯	⋯	25.7	25.6	25.4	25.4	19.7	19.5	18.5
θ_y/θ_x	0.14	0.16	⋯	⋯	6.3	6.23	5.90	5.22	⋯	⋯	⋯

from localized shear near the edges of the hinges and pads, while near a sample surface squeeze film effects become more important.

For the single axis levers, we find that the primary avenues for improving performance are reductions in pad thickness and pad area, although the latter tends to generate problems for locating the optical lever. Future simulations can explore stiffer cantilevers with higher frequency responses and lower low frequency noise. The main difficulty in using stiff levers is accidentally damaging of the sample during the approach. An extended analysis of the frequency and Q dependence of the dynamics while approaching a substrate may suggest new algorithms to make the approach robust. Simulations of gimbaled levers show that rotations about the orthogonal axes remain mostly independent, even at the resonance frequencies. This coupling is primarily intrinsic to the mechanics of the structure; however, external hydrodynamics slightly influence the coupling. Future studies will evaluate how best to emphasize the substrate induced coupling and minimize the bulk fluid induced coupling. Clearly, if the two resonance frequencies are moved further apart, there will be less coupling. The computations close to the surface for the gimbaled lever show the increased influence of the hydrodynamics on cross-axis coupling independent of any specific properties of the sample. The resonance frequencies and Q factors of the two modes decrease upon approach providing a useful monitor of the approach, but also limiting the bandwidth. The tip lengths or resonance frequencies can be adjusted to avoid overdamped modes when the lever is brought close to the sample plane.

ACKNOWLEDGMENTS

One of the authors (A.R.) acknowledges financial support for this research from the Sandia National Laboratories under Contract No. 623235 and another author (F.S.) acknowledges financial support from the National Science Foundation. The probes were fabricated at the Cornell NanoScale Facility.

[1] R. Raiteri, M. Grattarola, H. J. Butt, and P. Skladal, Sens. Actuators B **79**, 115 (2001).
[2] E. P. Wojcikiewicz, X. Zhang, and V. T. Moy, Biol. Proced. Online **6**, 1 (2004).
[3] Q. M. Zhang, J. Jaroniec, G. Lee, and P. E. Marszalek, Angew. Chem., Int. Ed. **44**, 2723 (2005).
[4] C. Spagnoli, A. Beyder, S. Besch, and F. Sachs, Rev. Sci. Instrum. (in press).
[5] M. S. Z. Kellermayer, L. Grama, A. Karsai, A. Nagy, A. Kahn, Z. L. Datki, and B. Penke, J. Biol. Chem. **280**, 8464 (2004).
[6] H. J. Janovjak, J. Struckmeier, and D. J. Muller, Eur. Biophys. J. **34**, 91 (2005).
[7] M. B. Viani, T. E. Schaffer, A. Chand, M. Rief, H. E. Gaub, and P. K. Hansma, J. Appl. Phys. **86**, 2258 (1999).
[8] A. Beyder and F. Sachs, Ultramicroscopy **106**, 838 (2006).
[9] A. Beyder, C. Spagnoli, and F. Sachs, Rev. Sci. Instrum. **77**, 056105 (2006).
[10] J. E. Sader, J. Appl. Phys. **84**, 64 (1998).
[11] C. P. Green and J. E. Sader, J. Appl. Phys. **92**, 6262 (2002).
[12] C. P. Green and J. E. Sader, Phys. Fluids **17**, 073102 (2005).
[13] S. Basak, A. Raman, and S. V. Garimella, J. Appl. Phys. **99**, 114906 (2006).
[14] ADINA, www.adina.com.
[15] S. Basak and A. Raman, Phys. Fluids **19**, 017105 (2007).
[16] MATLAB Online Documentation Set, The MathWorks, 2006.